UC San Diego
UC San Diego Previously Published Works

Title
Cerebral cavernous malformations proteins inhibit Rho kinase to stabilize vascular integrity

Permalink
https://escholarship.org/uc/item/83828200

Journal
Journal of Experimental Medicine, 207(4)

ISSN
0022-1007

Authors
Stockton, Rebecca A
Shenkar, Robert
Awad, Issam A
et al.

Publication Date
2010-04-12

DOI
10.1084/jem.20091258

Peer reviewed

Cerebral cavernous malformations proteins inhibit Rho kinase to stabilize vascular integrity

Rebecca A. Stockton,[1] Robert Shenkar,[2,3] Issam A. Awad,[2,3] and Mark H. Ginsberg[1]

[1]Department of Medicine, University of California, San Diego, La Jolla, CA 92093
[2]North Shore University Health System, Evanston, IL 60201
[3]University of Chicago Pritzker School of Medicine, Chicago, IL, 60637

Endothelial cell–cell junctions regulate vascular permeability, vasculogenesis, and angiogenesis. Familial cerebral cavernous malformations (CCMs) in humans result from mutations of *CCM2* (malcavernin, OSM, MGC4607), *PDCD10* (CCM3), or *KRIT1* (CCM1), a Rap1 effector which stabilizes endothelial cell–cell junctions. Homozygous loss of *KRIT1* or *CCM2* produces lethal vascular phenotypes in mice and zebrafish. We report that the physical interaction of KRIT1 and CCM2 proteins is required for endothelial cell–cell junctional localization, and lack of either protein destabilizes barrier function by sustaining activity of RhoA and its effector Rho kinase (ROCK). Protein haploinsufficient *Krit1*$^{+/-}$ or *Ccm2*$^{+/-}$ mouse endothelial cells manifested increased monolayer permeability in vitro, and both *Krit1*$^{+/-}$ and *Ccm2*$^{+/-}$ mice exhibited increased vascular leak in vivo, reversible by fasudil, a ROCK inhibitor. Furthermore, we show that ROCK hyperactivity occurs in sporadic and familial human CCM endothelium as judged by increased phosphorylation of myosin light chain. These data establish that KRIT1–CCM2 interaction regulates vascular barrier function by suppressing Rho/ROCK signaling and that this pathway is dysregulated in human CCM endothelium, and they suggest that fasudil could ameliorate both CCM disease and vascular leak.

CORRESPONDENCE
Mark H. Ginsberg:
mhginsberg@ucsd.edu

Abbreviations used: ANOVA, analysis of variance; CCM, cerebral cavernous malformations; cDNA, complementary DNA; FN, fibronectin; HUVEC, human umbilical vein endothelial cell; MLC, myosin light chain; pMLC, phosphorylated MLC; ROCK, Rho kinase; siRNA, small interfering RNA; SMC, smooth muscle cell; TBST, TBS-Tween.

Familial cerebral cavernous malformations (CCMs) disease results from autosomal dominant loss of function mutations in the genes *KRIT1* (CCM1), *CCM2* (malcavernin, MGC4607), or *PDCD10* (CCM3; Plummer et al., 2005). Homozygous null mutations are embryonic lethal, whereas heterozygosity predisposes to development of CCM lesions (Sahoo et al., 1999; Liquori et al., 2003); however, lesions may also arise sporadically. CCM lesions are dilated clusters of small vessels composed of fragile endothelium lacking underlying smooth muscle, with altered subendothelial extracellular matrix and no intervening neural parenchyma. Cerebral lesions exhibit defective endothelial cell–cell junctions and cause neurological deficits, seizures, and hemorrhagic stroke (Awad, 2005). Although some CCM patients also develop retinal and epidermal lesions, additional in vivo human phenotypes associated with heterozygosity have not been described, except for a description of abnormal growths in mesenchymal tissues (Ardeshiri et al., 2008).

CCM proteins are expressed in most tissues, including microvascular endothelium, but their intracellular functions are still not well characterized. We previously found that KRIT1 protein is localized to endothelial cell–cell junctions (Glading et al., 2007) and interacts with the membrane protein Heg1 (heart of glass 1; Kleaveland et al., 2009). Small interfering RNA (siRNA)–mediated depletion of KRIT1 led to junction disassembly and loss of β-catenin from the junctions, which is associated with increased monolayer permeability (Glading et al., 2007). KRIT1, CCM2, and CCM3 proteins physically interact (Zawistowski et al., 2005; Hilder et al., 2007a; Voss et al., 2007), which, in addition to their genetic relationship, suggests that Heg1 and these three proteins form a critical node in a signaling pathway regulating vascular development and endothelial

permeability. Moreover, these proteins interact with a variety of other potential signaling molecules. For example, KRIT1 binds to and is regulated by Rap1 (Serebriiskii et al., 1997; Gladding et al., 2007), a known stabilizer of endothelial cell–cell junctions (Cullere et al., 2005; Kooistra et al., 2005; Wittchen et al., 2005). The mechanism whereby this CCM protein complex regulates vascular functions is undefined.

We previously showed that KRIT1 knockdown in endothelial cells increases actin stress fibers, a morphology which led us to suggest that KRIT1 might suppress RhoA signaling, limiting actin-mediated contractility which contributes to endothelial junctional instability. In this paper, we report that both KRIT1 and CCM2 are negative regulators of RhoA and its effector Rho kinase (ROCK), thus limiting endothelial permeability in vitro and vascular leak. Pharmacological blockade of ROCK reversed both KRIT1 and CCM2 depletion–induced myosin light chain (MLC) phosphorylation, actin stress fiber formation, and endothelial monolayer permeability in vitro. In vivo, heterozygous $Krit1^{+/-}$ and $Ccm2^{+/-}$ mice, deficient in their respective encoded proteins, exhibited impaired pulmonary and cerebral vessel barrier function that was reversible by treatment with the ROCK inhibitor fasudil. Furthermore, isolated endothelium from multiple organs of both $Krit1^{+/-}$ and $Ccm2^{+/-}$ mice exhibited increased phosphorylated MLC (pMLC) and actin stress fiber content. Both sporadic and familial human CCM cerebral lesions displayed increased endothelial MLC phosphorylation, indicating that dysregulation of vascular RhoA-ROCK signaling is a feature of the human disease. Thus, KRIT1 and CCM2 regulate endothelial junctional stability and vascular barrier function by suppressing activation of the RhoA→ROCK pathway. This pathway is hyperactivated in human CCM endothelium and may contribute to lesion pathogenesis.

RESULTS
KRIT1 inhibition of RhoA and ROCK maintains endothelial barrier function
We previously showed that loss of KRIT1 leads to increased endothelial permeability associated with appearance of prominent stress fibers. Stress fiber development is often linked to increased RhoA activity (Sun et al., 2006). KRIT1 depletion by siRNA caused a 3.5-fold increase in activated RhoA in cultured human umbilical vein endothelial cells (HUVECs; Fig. 1 A). The specificity of KRIT1 siRNA effect was confirmed by transfection with control siRNA and reconstitution with siRNA-resistant KRIT1. Total RhoA expression was unchanged in all conditions (Fig. 1 B). Thus, endogenous endothelial KRIT1 inhibits RhoA activity.

ROCK is a RhoA effector mediating actin stress fiber formation in part by increasing MLC phosphorylation and, consequently, cellular contractility. MLC is a ROCK substrate. ROCK also phosphorylates and inhibits myosin phosphatase (Shimokawa and Takeshita, 2005) permitting sustained MLC phosphorylation. As a measure of ROCK

activity, we stained KRIT1 siRNA–treated HUVEC for pMLC and evaluated stress fiber content (Fig. 1 C). KRIT1-depleted cells manifested increased pMLC staining, particularly at cell–cell junctions and along stress fibers, which were increased in number. Both effects of KRIT1 siRNA were reversed by a ROCK inhibitor, H-1152, and by a second ROCK inhibitor, Y27632 (Fig. S1). Staining for phosphorylation of a second ROCK substrate, myosin phosphatase binding subunit, produced similar results (Fig. S1). Western blotting for KRIT1 protein verified the degree of KRIT1 depletion by siRNA (Fig. 1, B and D). Inhibition of ROCK had no effect on the degree of KRIT1 depletion. Of greater significance, ROCK inhibition by H-1152 reversed effects of KRIT1 depletion on monolayer permeability in HUVEC (Fig. 1 E). Thus, suppression of RhoA activity and its downstream effector ROCK enables KRIT1 to maintain stability of endothelial cell junctions.

KRIT1 haploinsufficiency induces ROCK–mediated vascular leak
$KRIT1^{+/-}$ humans are at risk of developing CCMs, lesions which have defective endothelial cell–cell junctions. We found that $Krit1^{+/-}$ mice expressed half the WT levels of KRIT1 protein in pulmonary and brain lysates (Fig. 2, A and B). $Krit1^{+/-}$ mice exhibited increased basal vascular leak, as measured by Evan's blue dye extravasation, and greater LPS–induced leak in both brain and pulmonary vessels (Fig. 2, C and D). Similar differences between WT and heterozygous mice were observed in brain and lung edema assays of wet/dry weight, a secondary index of vascular leak (Fig. 2, E and F; Wilson et al., 2007). We tested brain and lung because both are highly vascular. Although clinically recognized CCM lesions are largely cerebral (Gault et al., 2006), these data suggest that $Krit1^{+/-}$ mice suffer from more widespread vascular endothelial defects. This idea was supported by increased pMLC content of endothelial cells isolated from multiple organs of $Krit1^{+/-}$ mice (Fig. 3 A). Furthermore, KRIT1 protein was expressed at similar levels in endothelial cells from all organs evaluated, with endothelial cells from heterozygous mice expressing one-half as much as those from WT mice (Fig. 3 A and Fig. S2). Increased pMLC staining, actin stress fibers, and monolayer permeability were seen in pulmonary endothelial cells cultured from $Krit^{+/-}$ mice (Fig. 3, B and C). Thus, hemizygous deficiency of KRIT1 leads to haploinsufficiency and generalized vascular barrier dysfunction, which is reversible by a ROCK inhibitor in vivo and in vitro.

KRIT1 or CCM2 deficiency is associated with increased pMLC in human cerebral CCM lesions
$KRIT1$ hemizygosity in humans is associated with development of dilated capillary clusters with fragile endothelium, which are known to have defective cell–cell junctions and propensity to leak (Clatterbuck et al., 2001; Gault et al., 2006). Our findings led us to evaluate resected human CCM lesions by immunohistochemistry for increased pMLC as an index of ROCK activity. Familial and sporadic cerebral lesions were stained for KRIT1 and CCM2 to evaluate protein expression. Absence of protein

coded for by the mutated gene has been observed in lesions from heterozygous humans (Pagenstecher et al., 2009) and is ascribable to a "second hit" in lesion endothelial cells (Akers et al., 2009). Both KRIT1 and CCM2 were detectable by immunohistochemistry in control endothelium from human anterior temporal lobe tissue removed surgically for epilepsy. CCM lesion endothelium from a sporadic

patient was deficient in KRIT1 protein, and a lesion from a familial patient, genotyped as a *Ccm2* mutation, lacked endothelial CCM2 (Fig. S3). Both the sporadic and the familial lesions exhibited dramatic increases in endothelial pMLC when compared with control brain tissue (Fig. 4 A). The control brain sample showed pMLC in vessel medial smooth muscle cell (SMC) layer, as would be expected, because
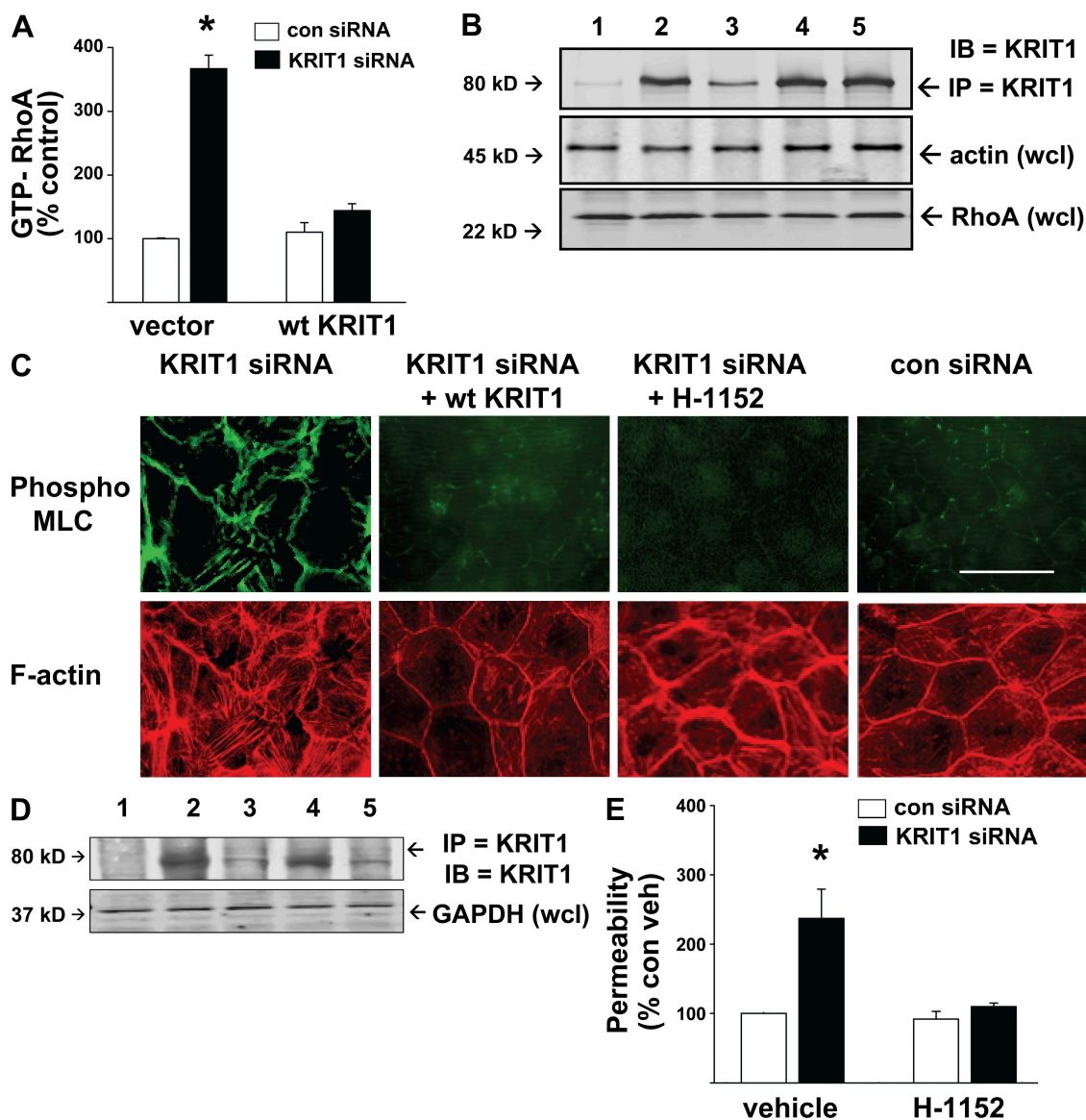

Figure 1.   **KRIT1 inhibits RhoA and its effector ROCK to reduce MLC phosphorylation and permeability in vitro.** (A) HUVECs treated with control or KRIT1 siRNA were evaluated for RhoA activity. KRIT1-depleted cells had a 3.5-fold increase in GTP-RhoA compared with control, reversible by cotransfection with WT KRIT1 bearing a knockdown-resistant silent mutation. Error bars are means and SE of $n = 6$. *, $P < 0.001$ compared with vector-only control siRNA. (B) Total RhoA is shown by immunoblotting, and equal protein content per sample is shown by actin loading. KRIT1 siRNA efficacy is shown by immunoprecipitated KRIT1 content. 1, control IP with mouse IgG; 2, control siRNA; 3, KRIT1 siRNA; 4, control siRNA + KRIT1 complementary DNA (cDNA); 5, KRIT1 siRNA + KRIT1 cDNA. (C) KRIT1 depletion increased MLC phosphorylation and f-actin stress fiber content. Reconstitution with WT KRIT1 prevented pMLC increase and reduced stress fibers. Treatment of KRIT1-depleted cells with ROCK inhibitor H-1152 also prevented MLC phosphorylation and stress fiber formation, indicating that ROCK acts downstream of KRIT1. Bar, 50 µm. (D) siRNA efficacy is shown by Western blot probed for KRIT1. 1, control IgG IP; 2, control siRNA; 3, KRIT1 siRNA; 4, KRIT1 siRNA+ KRIT1 cDNA; 5, KRIT1 siRNA + H-1152. (E) KRIT1 depletion increases HUVEC monolayer permeability in Transwell assays. The increase is reversible by H-1152 treatment, indicating that KRIT1 functions to inhibit ROCK-mediated monolayer leak. Error bars are means ± SE of $n = 6$. *, $P < 0.001$ compared with control siRNA

ROCK signaling is a regulator of vascular SMC contractility (Berridge, 2008), but there was little endothelial staining. High magnification of a familial lesion vessel demonstrated strong pMLC staining in the endothelium (Fig. 4 B). These data support the concept that CCM is largely a disorder of endothelial cells (Glading et al., 2007; Boulday et al., 2009) and indicate

that the RhoA–ROCK pathway is hyperactivated in human lesion endothelium.

CCM2 depletion increases ROCK activity in vitro

KRIT1 and CCM2 physically associate (Zawistowski et al., 2005; Hilder et al., 2007a; Zhang et al., 2007), and
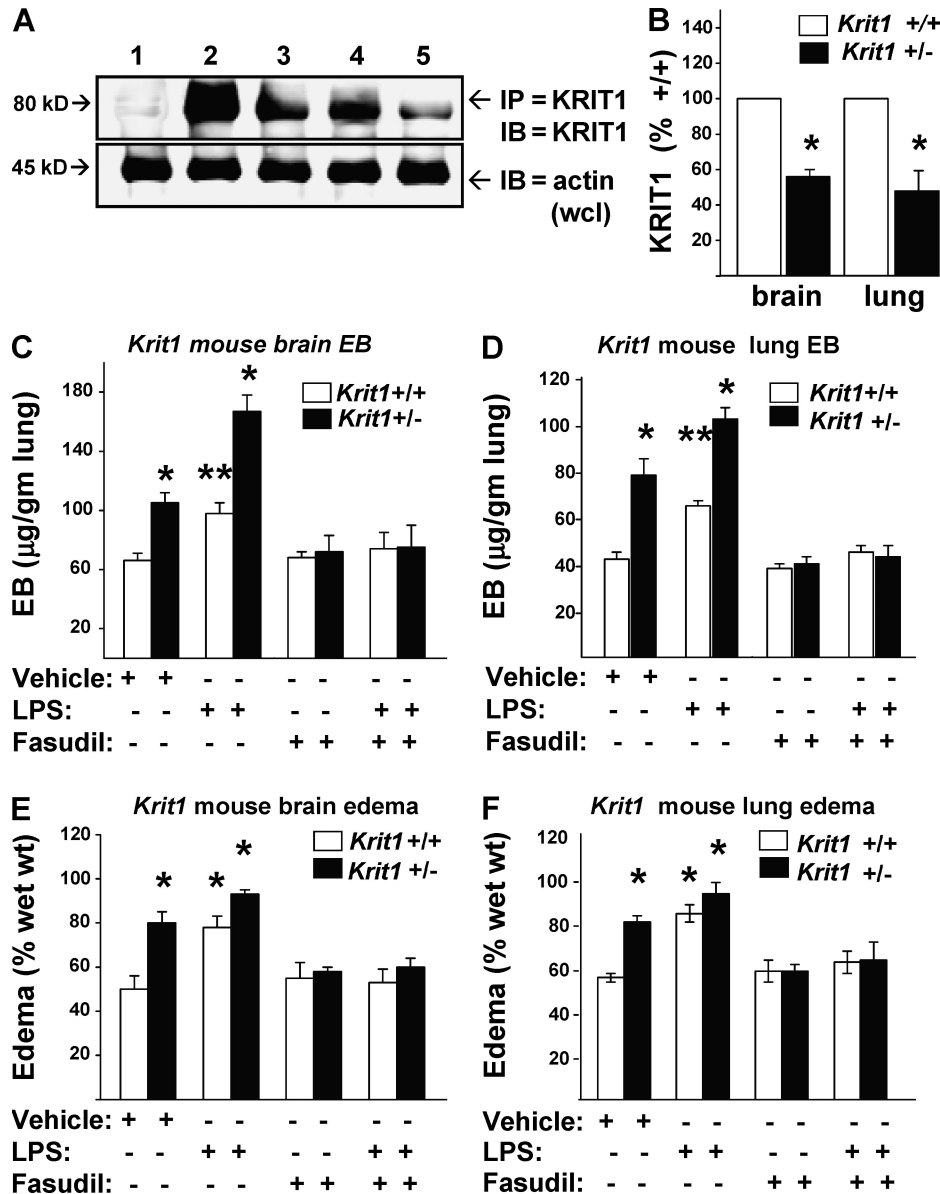

Figure 2. **KRIT1 protein haploinsufficiency increases ROCK–mediated vascular leak in vivo.** (A) $Krit1^{+/-}$ mice have one-half the amount of KRIT1 protein in lung and brain as $Krit1^{+/+}$ mice. 1, control mouse IgG IP; 2, $Krit1^{+/+}$ lung; 3, $Krit1^{+/+}$ brain; 4, $Krit1^{+/-}$ lung; 5, $Krit1^{+/-}$ brain lysates. (B) Densitometry of blots in A shows a 50% reduction in KRIT1 in $Krit1^{+/-}$ lysates. Error bars are means ± SE ($n = 3$). *, $P < 0.03$ compared with $Krit1^{+/+}$. (C) $Krit1^{+/-}$ mice had significantly greater basal and LPS-induced Evan's blue dye leak in brain. Error bars are means and SE of $n = 6$ mice. *, $P < 0.01$; **, $P < 0.04$ compared with vehicle-treated $Krit1^{+/+}$ mice. Fasudil reduced leak in the $Krit1^{+/-}$ mice. (D) Lungs were collected from animals treated as in C and evaluated for dye extravasation. Basal and LPS-induced lung leak were also reversed by fasudil treatment. Error bars are means ± SE ($n = 6$). *, $P < 0.01$; **, $P < 0.03$ compared with $Krit1^{+/+}$. (E) Brain edema (difference in wet weight vs. dry weight) was also tested under the same conditions. Brains were weighed, desiccated, and reweighed. Means and SE of data from six animals are shown. Brain edema was increased in $Krit1^{+/-}$ mice and was reduced by fasudil treatment. Error bars are means ± SE ($n = 6$). *, $P < 0.01$ compared with $Krit1^{+/+}$. (F) $Krit1^{+/-}$ mice also had increased pulmonary edema, which was diminished by fasudil treatment. Error bars are means ± SE ($n = 6$). *, $P < 0.01$ compared with $Krit1^{+/+}$.

homozygous null mutations in either gene result in similar lethal vascular and cardiac phenotypes in mice and zebrafish. As shown in Fig. 4, we demonstrated that a CCM2-deficient human cerebral CCM exhibited increased endothelial pMLC.

Depletion of CCM2 was recently reported to increase RhoA-GTP loading in vitro (Crose et al., 2009; Whitehead et al., 2009), suggesting that CCM2 deficiency might also activate the Rho–ROCK pathway to disrupt endothelial
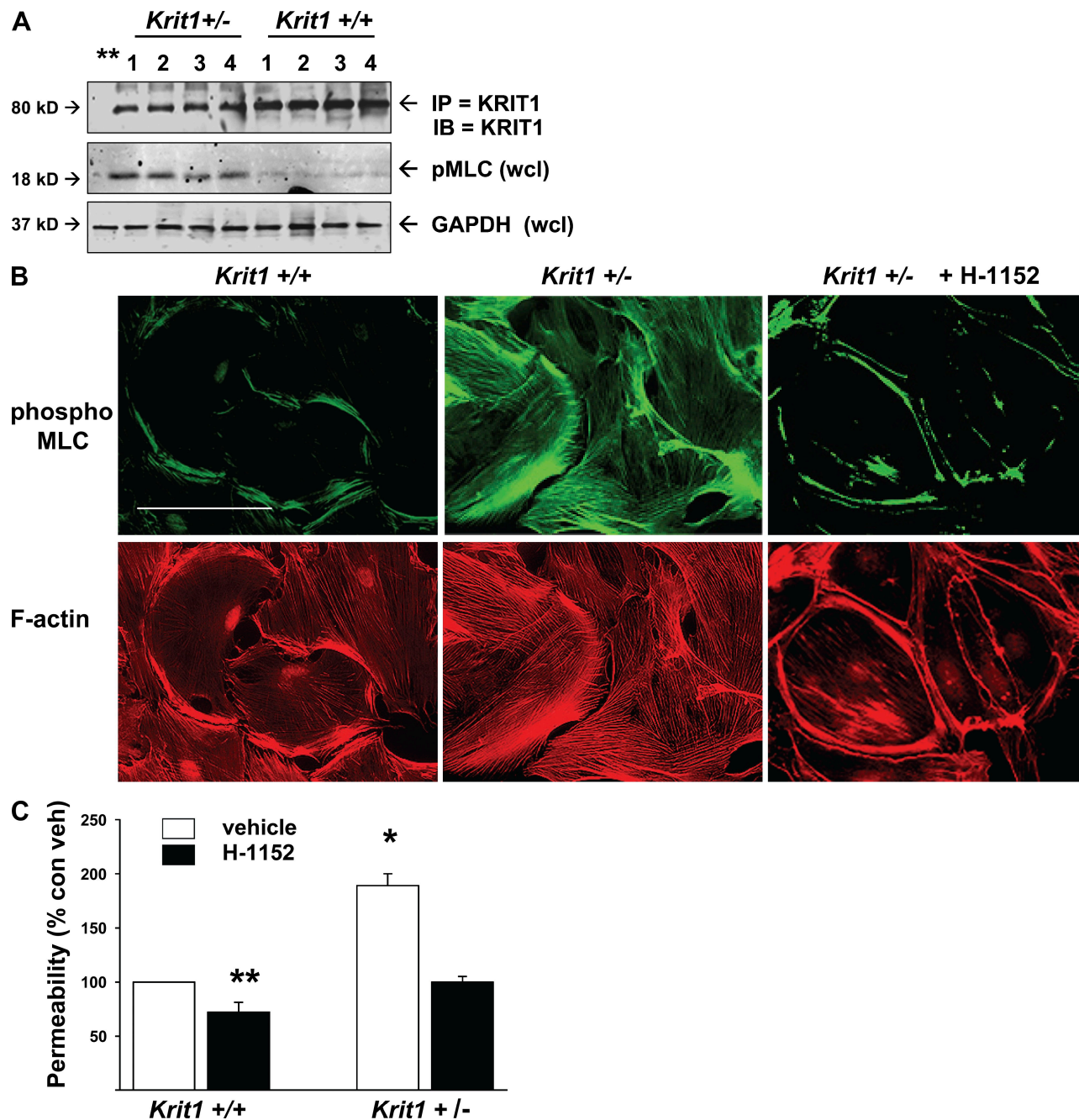

Figure 3. *Krit1+/−* **mouse endothelial cells have increased in vivo and in vitro pMLC and in vitro leak.** (A) Endothelial cells were isolated from *Krit1+/+ and Krit1+/−* mouse brain, lung, liver, and kidney as described in Materials and methods, lysed, and Western blotted for immunoprecipitated KRIT1 protein and for pMLC in whole cell lysate. 1, brain; 2, lung; 3, liver; 4, kidney. Endothelial cells from *Krit1+/−* mice had similar KRIT1 protein expression in all organs but ∼1/2 the amount seen in *Krit1+/+* mice. Endothelial cells from all organs in *Krit1+/−* mice exhibited increased pMLC content in vitro. (B) Isolated pulmonary endothelial cells grown on FN-coated coverslips were also stained for pMLC and f-actin content. *Krit1+/−* cells exhibited an increase in both. Bar, 50 µm. (C) In vitro permeability assay of isolated pulmonary endothelial cells. *Krit1+/−* endothelial monolayers were twofold more permeable than WT. Permeability was reduced by the ROCK inhibitor H-1152. Error bars are means ± SE ($n = 6$). *, $P < 0.001$; **, $P < 0.05$ compared with vehicle-treated *Krit1+/+*.
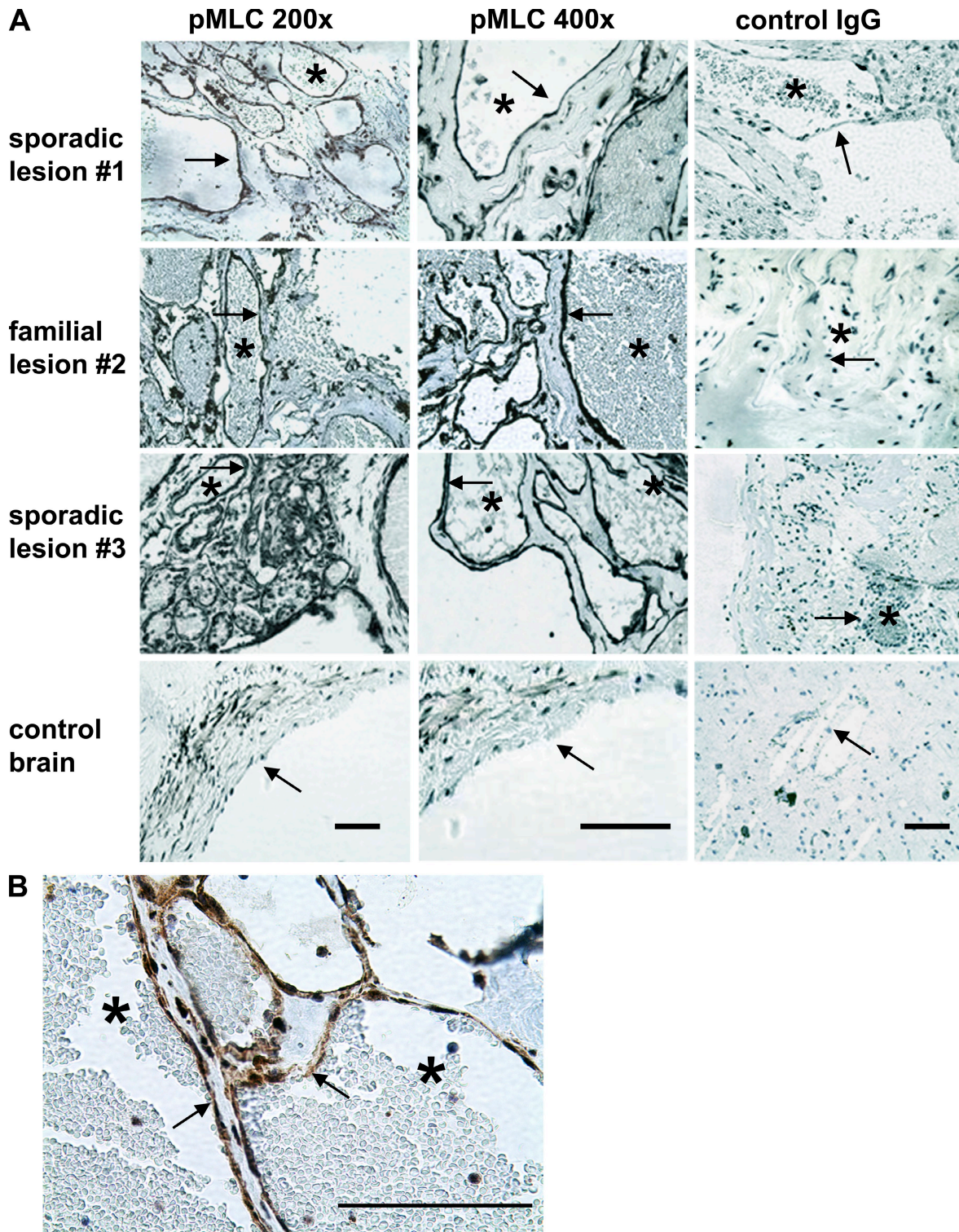
Figure 4. KRIT1 haploinsufficiency increases ROCK activity in human cerebral lesion endothelium. (A) Human CCM cerebral lesions were compared with nonlesion control brain tissue. Slides were processed as described in Materials and methods, stained with anti-pMLC as an index of ROCK activation, and counterstained with hematoxylin. Control antibody stains are with rabbit IgG. The left and center columns are stained for pMLC, and the right column is stained with control antibody. Bars, 500 µm. The CCM lesions are clusters of distended capillaries lacking SMC underlayer. Arrows indicate cavern endothelial cells; asterisks mark lumen of a typical expanded lesion vessel. The control non-CCM brain tissue panel shows an arteriole in cross section, exhibiting pMLC in SMC subendothelial layer, but little in endothelial cells (arrow) facing vessel lumen. Sporadic lesion #1 is KRIT1 protein deficient (Fig. S3). Familial lesion #2 is CCM2 deficient (Fig. S3) and has equally robust endothelial pMLC staining. (B) Magnified view of familial lesion #2 endothelium.

cell–cell junctions. We therefore evaluated CCM2 effects on RhoA-ROCK signaling in vitro. siRNA depletion of CCM2 increased Rho-GTP levels and pMLC staining in HUVEC to a similar extent as KRIT1 depletion and was reversed by coexpression of siRNA-resistant CCM2 (Fig. 5, A and C). Total RhoA expression was equivalent in all conditions (Fig. 5 B). Similar effects were observed in staining for a second ROCK substrate, phospho-MYPT1 (Fig. S1). The effects of CCM2 depletion were reversed by treatment with ROCK inhibitors H-1152 or Y27632. Finally, CCM2 depletion caused increased HUVEC mono-

layer permeability reversible by ROCK inhibition (Fig. 5 D). Thus, like KRIT1, CCM2 acts upstream of ROCK to regulate endothelial permeability.

CCM2 haploinsufficiency induces ROCK–mediated vascular leak

To learn whether in vitro CCM2-associated endothelial permeability was mirrored by defects in vascular barrier function, as was seen with $Krit1^{+/-}$ mice, we also evaluated CCM2 protein expression in $Ccm2^{+/+}$ and $Ccm2^{+/-}$ mice. $Ccm2^{+/-}$ brain and lung had approximately half the CCM2 protein content of WT organs (Fig. 6, A and B). Vascular leak of
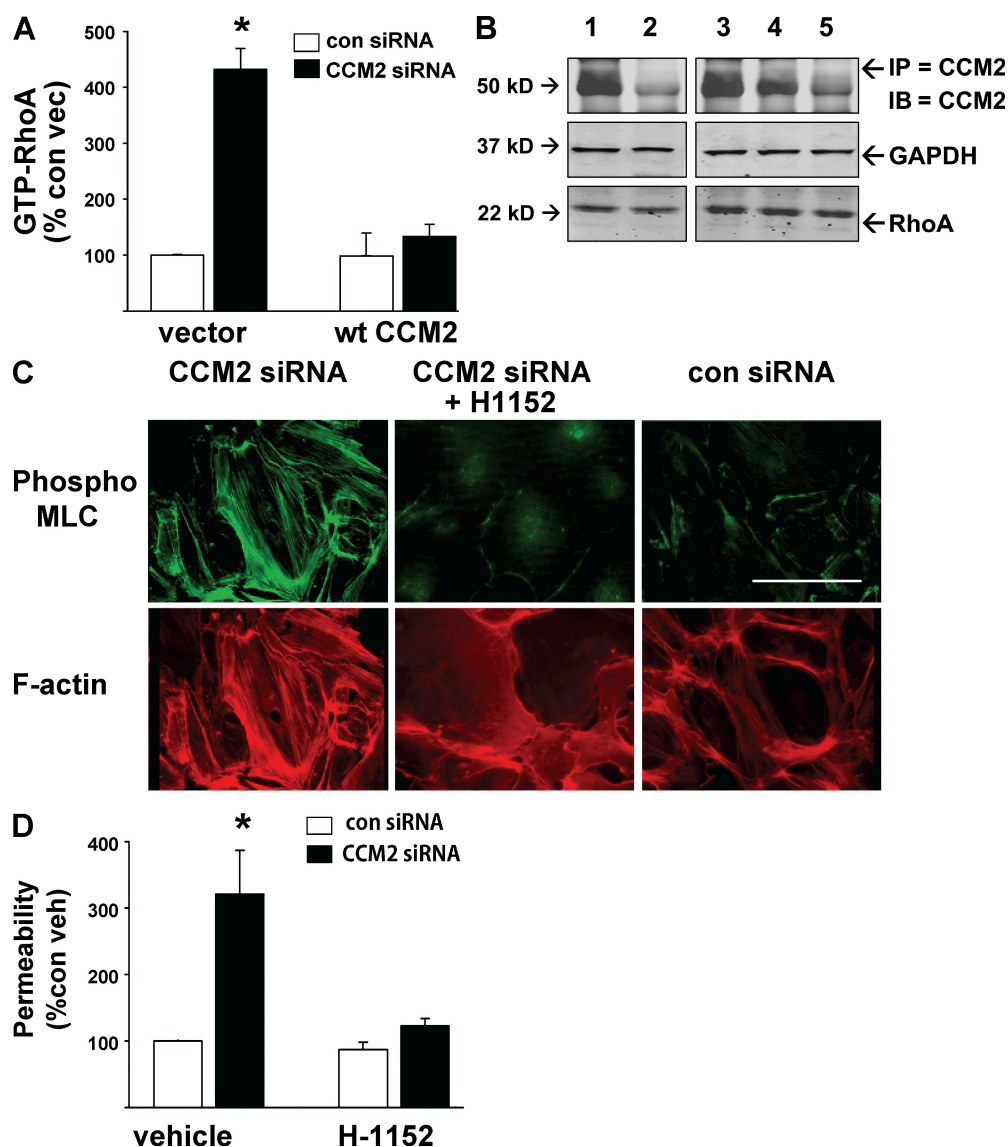

Figure 5. **CCM2 depletion increases RhoA and ROCK activity in vitro.** (A) HUVECs were treated with CCM2 or control siRNA, with or without WT CCM2 bearing a silent mutation resistant to knockdown. Depletion of CCM2 produced a four- to sixfold increase in GTP-RhoA, reversible by cotransfection with WT CCM2. Error bars are means ± SE ($n = 6$). *, $P < 0.001$ compared with control siRNA. (B) Total RhoA is equal in all treatments. Equal sample protein is shown by GAPDH. CCM2 knockdown and reconstitution efficacy are shown by immunoprecipitated CCM2. 1, vector + control siRNA; 2, vector + CCM2 siRNA; 3, control siRNA + WT CCM2 cDNA; 4, CCM2 siRNA + WT CCM2 cDNA; 5, control rabbit IgG IP. (C) CCM2 depletion by siRNA increases pMLC and stress fiber content of HUVEC, reversible by treatment with ROCK inhibitor H-1152. Bar, 50 μm. (D) As previously seen with KRIT1, CCM2 presence is required for suppression of ROCK-mediated monolayer permeability. Error bars are means ± SE ($n = 4$). *, $P < 0.001$ compared with vehicle-treated control siRNA.

Evan's blue dye was increased in brain and lung of $Ccm2^{+/-}$ animals compared with WT littermates, both in basal conditions and in response to LPS challenge (Fig. 6, C and D). Organ edema was proportionately increased as well (Fig. 6, E and F). Increased permeability and organ edema were reversed by treatment with fasudil (Fig. 6, C–F). As was seen with $Krit^{+/-1}$ mice, isolated mouse brain, lung, liver, and kidney endothelial cells expressed equivalent amounts of CCM2

protein, with $Ccm2^{+/-}$ mice expressing one-half as much as $Ccm2^{+/+}$ mice (Fig. 7 A). Like the $Krit1^{+/-}$ mice, isolated endothelial cells from all organs of $Ccm2^{+/-}$ mice showed increased pMLC content (Fig. 7, A and B) and increased monolayer permeability (Fig. 7 C). Thus, CCM2 deficiency phenocopies effects of KRIT1 deficiency on dysregulation of Rho-ROCK signaling and resulting vascular barrier dysfunction.
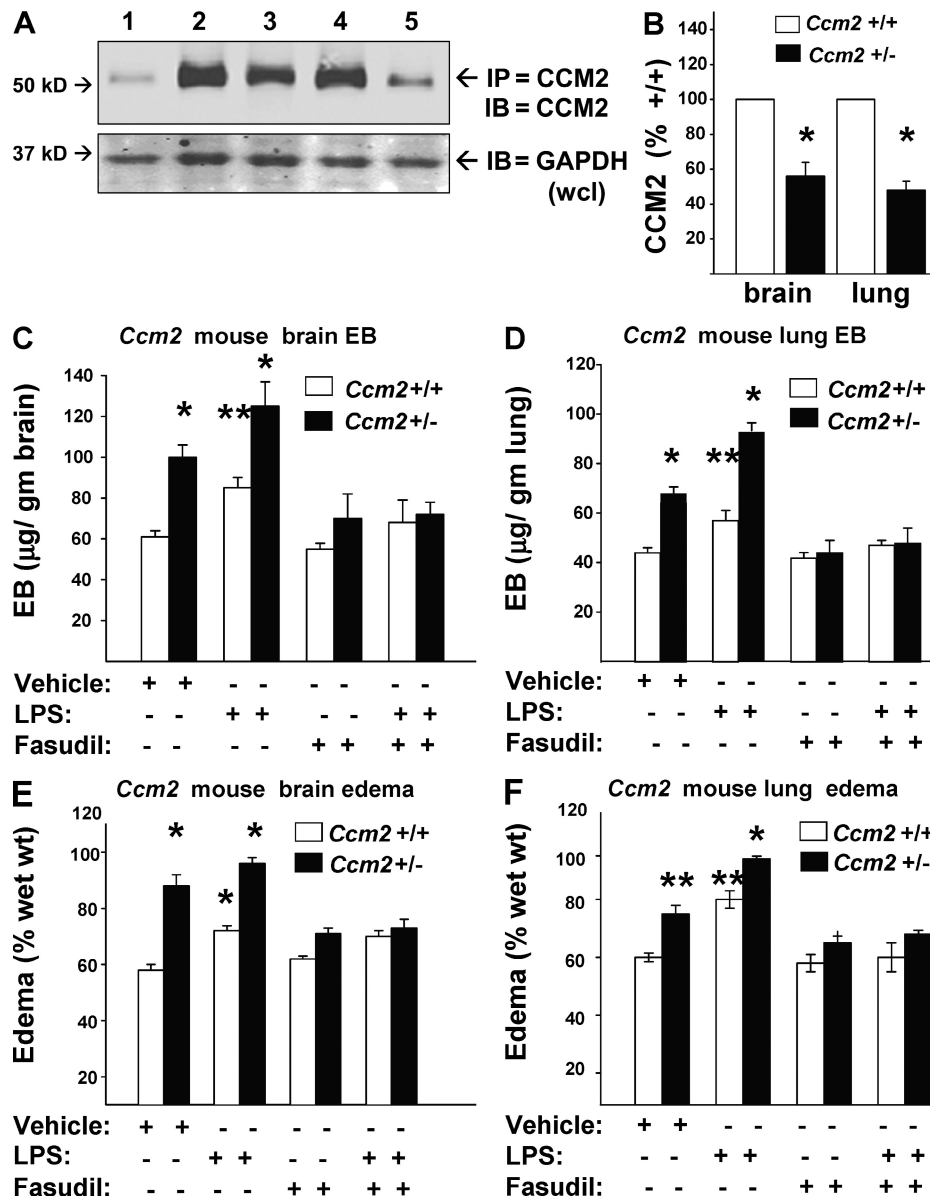

Figure 6. **CCM2 protein haploinsufficiency increases ROCK–mediated vascular leak.** (A) Lung and brain lysates of $Ccm2^{+/+}$ and $Ccm2^{+/-}$ mice evaluated for CCM2 protein content show a 50% protein reduction in $Ccm2^{+/-}$. 1, control mouse IgG IP; 2, $Ccm2^{+/+}$ lung; 3, $Ccm2^{+/+}$ brain; 4, $Ccm2^{+/-}$ lung; 5, $Ccm2^{+/-}$ brain lysates. (B) Densitometry shows one-half CCM2 protein expression in heterozygous mouse lung and brain compared with WT. Error bars are means ± SE ($n = 3$). *, P < 0.01 compared with same organ of $Ccm2^{+/+}$ mouse. (C) $Ccm2^{+/+}$ and $Ccm2^{+/-}$ mice were evaluated for basal and LPS-induced cerebral vascular leak as described in Fig. 2. $Ccm2^{+/-}$ mice had significantly greater basal and induced leaks, reversible by ROCK inhibition with fasudil. Error bars are means ± SE ($n = 6$). *, P < 0.01; **, P < 0.03 compared with vehicle-treated $Ccm2^{+/+}$. (D) Similarly, pulmonary vascular leak was increased in $Ccm2^{+/-}$ mice and was also reduced by fasudil. Error bars are means ± SE ($n = 6$). *, P <0.01; **, P < 0.04 compared with vehicle-treated $Ccm2^{+/+}$. (E and F). Brain and lung edema in $Ccm2^{+/-}$ mice were increased, reversible by fasudil treatment. Error bars are means ± SE ($n = 6$). *, P < 0.01; **, P < 0.02 compared with vehicle-treated $Ccm2^{+/+}$ for both panels.

Physical interaction of KRIT1 with CCM2 is required for suppression of ROCK–mediated permeability

CCM2 mutations that inhibit its association with KRIT1 are linked to CCM disease in humans (Plummer et al., 2006; Liquori et al., 2007), suggesting that physical interaction of these proteins is important in their biological functions. In this paper, we have shown that CCM2 and KRIT1 both influence vascular barrier function by inhibiting activity of RhoA and its effector ROCK. To test whether physical interaction of KRIT1 and CCM2 modulates RhoA-ROCK signaling,
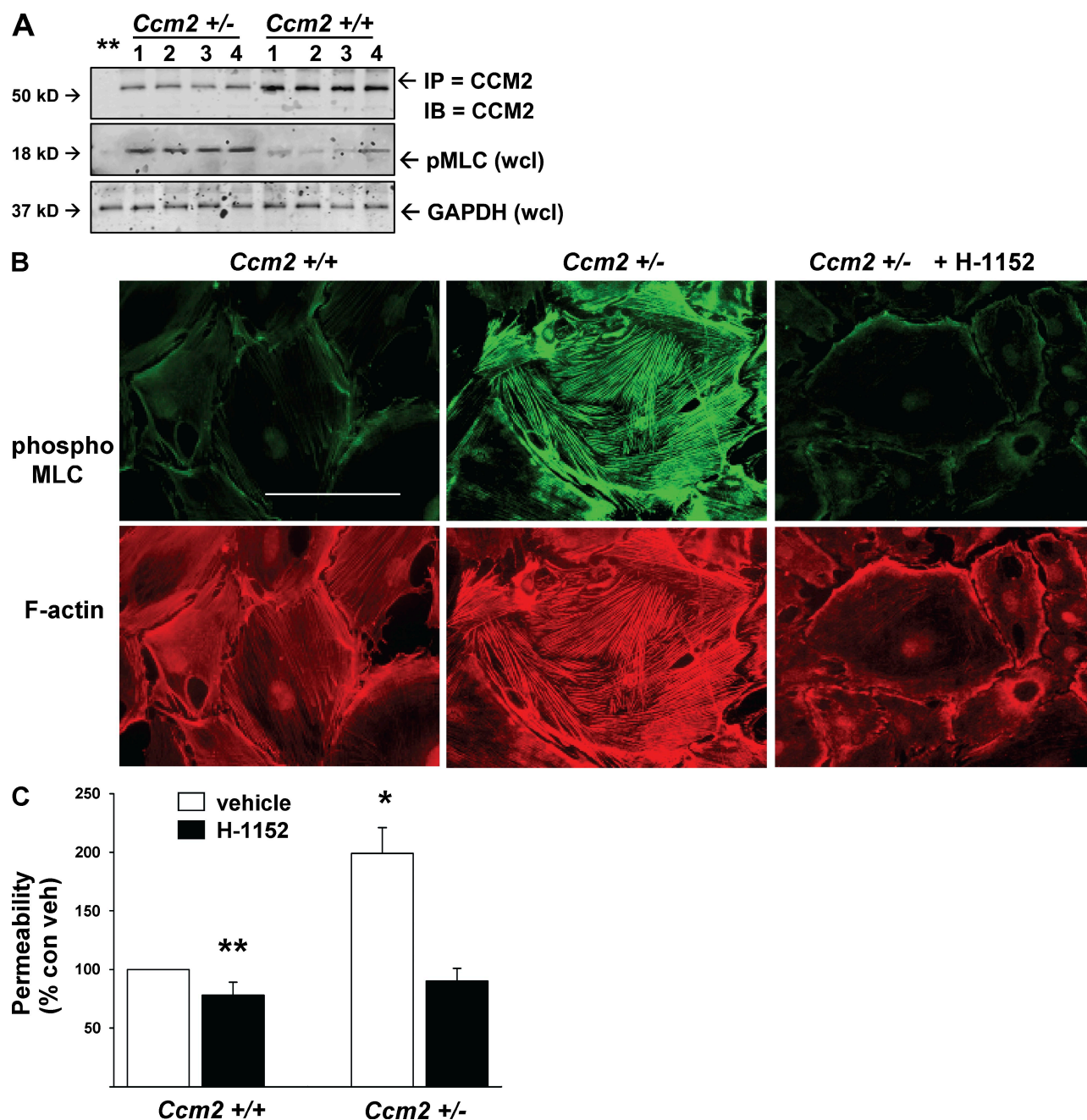

Figure 7. *Ccm2⁺/⁻* mouse endothelial cells exhibit increased pMLC in vivo and in vitro. (A) Endothelial cells isolated from *Ccm2⁺/⁺* and *Ccm2⁺/⁻* mouse brain, lung, liver, and kidney were lysed and probed for CCM2 protein and pMLC content. 1, brain; 2, lung; 3, liver; 4, kidney. Endothelial cells from all organs have equivalent expression of CCM2 protein; however, *Ccm2⁺/⁻* endothelial cells express 50% as much CCM2 as those from *Ccm2⁺/⁺* mice. *Ccm2⁺/⁻* mouse endothelial cells exhibited increased pMLC content compared with WT. (B) Pulmonary endothelial cells were probed for pMLC and actin structure in vitro. Increased MLC phosphorylation and stress fiber content are seen in *Ccm2⁺/⁻* cells. Bar, 50 µm. (C) *Ccm2⁺/⁻* endothelial cells exhibit increased monolayer permeability reversible by treatment with ROCK inhibitor H-1152. Error bars are means ± SE (n = 6). *, P < 0.001; **, P < 0.05 compared with vehicle-treated *Ccm2⁺/⁺* cells.
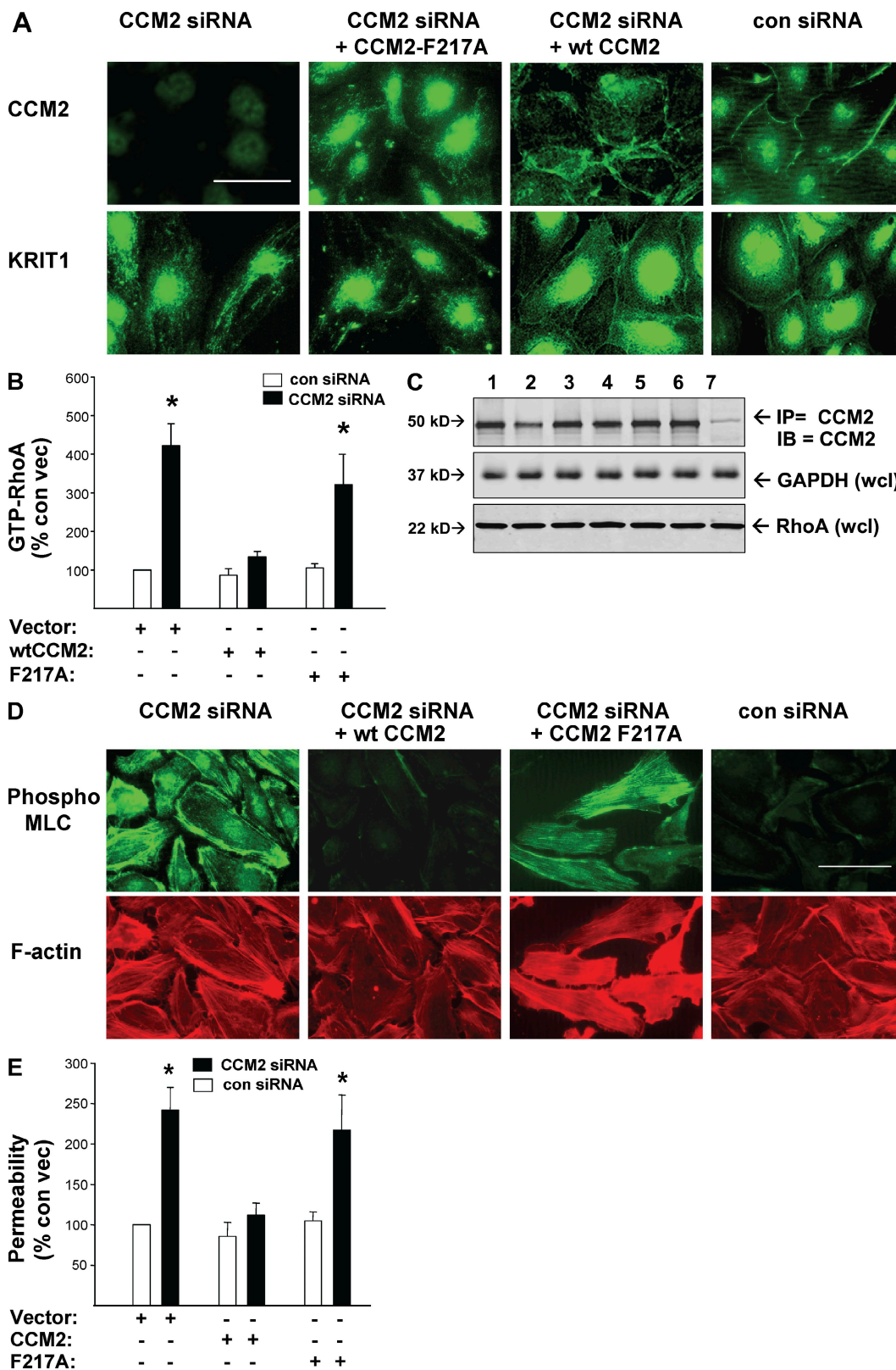
Figure 8. Physical interaction of CCM2 and KRIT1 is required for their endothelial junctional localization and for inhibition of RhoA→ROCK–mediated permeability. HUVECs were transfected with siRNA to deplete endogenous CCM2 and reconstituted with either WT CCM2 or CCM2-F217A, a mutation which abrogates CCM2 binding to KRIT1. Both WT CCM2 and CCM2-F217A constructs bear silent mutations conferring resistance to CCM2 siRNA. (A) Endogenous CCM2 and KRIT1 protein are localized to HUVEC endothelial cell–cell junctions in cells treated with control siRNA. CCM2

we first asked whether CCM2 is an endothelial junctional protein because previous studies reached divergent conclusions about CCM2 localization (Petit et al., 2006; Seker et al., 2006; Kleaveland et al., 2009), possibly as a result of staining of overexpressed recombinant proteins or differences in staining technique. Anti-CCM2 antibody stained endogenous CCM2 in HUVEC cell–cell junctions, which is consistent with its physical association with KRIT1 (Fig. 8 A). Furthermore, CCM2 depletion led to loss of KRIT1 from the cell–cell junctions. We used CCM2 siRNA to deplete HUVEC of endogenous CCM2 and then reconstituted with CCM2-F217A, a mutation which renders CCM2 unable to physically interact with KRIT1 (Zawistowski et al., 2005; Hilder et al., 2007a,b). CCM2 reconstitutions were equivalent in all transfections (Fig. 8 C). CCM2-F217A did not suppress RhoA activity (Fig. 8 B), nor did it restore the junctional localization of KRIT1 (Fig. 8 A). To evaluate further effects on ROCK activity and function, we probed CCM2 siRNA–depleted HUVEC for pMLC, actin stress fibers, and measured monolayer permeability. Reconstitution with CCM2-F217A failed to prevent MLC phosphorylation increase and stress fiber accumulation (Fig. 8 D), nor did it prevent increased permeability (Fig. 8 E). These data indicate that physical interaction of KRIT1 and CCM2 protein is required for KRIT1 junctional localization and for suppression of RhoA and ROCK activity to maintain vascular barrier function.

DISCUSSION

KRIT1 and CCM2 have been shown separately to regulate vasculogenesis (Whitehead et al., 2004, 2009; Kleaveland et al., 2009). Our earlier work identified KRIT1 as a Rap1 effector that is localized to endothelial cell–cell junctions in vitro and is required for junctional stability to limit monolayer permeability (Glading et al., 2007). In this paper, we establish a signaling pathway whereby KRIT1 regulates vascular permeability. KRIT1 interacts with CCM2 to stabilize endothelial cell–cell junctions, and they conjointly suppress RhoA activity and, thus, activation of the RhoA effector ROCK. We show that hemizygous deficiency of either KRIT1 or CCM2 leads to ROCK-mediated vascular leak in mice, suggesting much more widespread consequences of hemizygous deficiency of these proteins than previously appreciated. This vascular leak is reversible by treatment with a ROCK inhibitor, fasudil, an agent in clinical use. Furthermore, we find increased phosphorylation of the ROCK

substrate MLC in the endothelium of human CCM lesions associated with lack of either KRIT1 or CCM2. Thus, we define a mechanism by which KRIT1 interaction with CCM2 stabilizes endothelial cell junctions, we report that haploinsufficiency of either of these proteins leads to vascular leak in mice and dysregulated cerebral endothelial ROCK signaling in humans, and we identify fasudil as a potential therapy for CCM disease.

These studies indicate that a signaling module of KRIT1 and CCM2 acts as a negative regulator of RhoA, thereby limiting ROCK activity downstream. We show in this paper that CCM2, like KRIT1, localizes to endothelial junctions, and its direct physical interaction with KRIT1 is required for maintenance of endothelial junctional stability by suppressing ROCK activity. Binding of KRIT1 to CCM2 leads to KRIT1 transport out of the nucleus (Zawistowski et al., 2005). Once in the cytosol, KRIT1 can interact with junctional components, such as β-catenin (Glading et al., 2007) or Heg1 (Kleaveland et al., 2009), to recruit it to cell–cell junctions. Depletion of either KRIT1 or CCM2 by in vitro siRNA increased RhoA-GTP, confirming previous results showing that depletion of CCM2 leads to increased RhoA activity (Crose et al., 2009; Whitehead et al., 2009). Importantly, we show that reconstitution with WT CCM2, but not with a CCM2 mutant unable to interact with KRIT1, reverses the effects of CCM2 depletion, emphasizing that KRIT1 and CCM2 act as a complex. CCM2 interaction enables KRIT1 translocation from nucleus to plasma membrane in nonendothelial cells (Zawistowski et al., 2005), and we find that depletion of CCM2 leads to mislocalization of KRIT1 from endothelial cell–cell junctions. Thus, it is likely that the two proteins interact for sustained localization at junctional membranes, where they could regulate RhoA activity by influencing Rho GEFs or GAPs. Recently, Crose et al. (2009) found that CCM2 interacts with Smurf1, an E3 ubiquitin ligase, leading to reduced RhoA expression in an endothelial cell line; however, we saw no differences in total RhoA as a consequence of CCM2 or KRIT1 depletion in primary endothelial cells. Alternatively, CCM2 is a scaffold for MEKK3, p38 MAPK, and Rac1 (Uhlik et al., 2003; Fong et al., 2007; Hilder et al., 2007b). Rac1 activity counters RhoA-mediated stress fiber formation and stabilizes microvascular barrier function, although Rac1 can itself also mediate barrier disruption (Wójciak-Stothard et al., 2001, 2005; van Wetering et al., 2002;

depletion by siRNA causes KRIT1 loss from junctions. Reconstitution of depleted endogenous CCM2 by transfection with CCM2-F217A does not restore junctional localization either to the mutant CCM2 or to endogenous KRIT1. Reexpressed WT CCM2 is junctional and permits endogenous KRIT1 junctional localization. (B) CCM2-F217A reconstitution of endogenous CCM2 depletion fails to suppress RhoA activity, whereas reconstitution with WT CCM2 limits RhoA activity. Error bars are means ± SE ($n = 4$). *, $P < 0.01$ compared with vector-treated control siRNA. (C) Transfection and knockdown efficacy for A and B is shown by Western blotting for CCM2 and total RhoA content. Equal loading is shown by staining for GAPDH. 1, vector; 2, vector + CCM2 siRNA; 3, CCM2 cDNA; 4, CCM2 cDNA$^+$ CCM2 siRNA; 5, CCM2-F217A cDNA; 6, CCM2-F217A cDNA + CCM2 siRNA; 7, control rabbit IgG IP. (D) CCM2 depletion causes increased pMLC and actin stress fiber content, reversible by reconstitution with WT CCM2 but not by CCM2-F217A, indicating a requirement for CCM2-KRIT1 physical interaction for suppressing ROCK activity. Bar, 50 µm. (E) CCM2 depletion-induced hyperpermeability is not reversible by CCM2-F217A reconstitution. Error bars are means ± SE ($n = 6$). *, $P < 0.001$ compared with control siRNA.

Stockton et al., 2004, 2007; Gavard and Gutkind, 2006; Tan et al., 2008).

RhoA has multiple effectors but its regulation of vascular contractility is largely accomplished through ROCK. ROCK-mediated induction of endothelial permeability occurs in response to a variety of cytokines and growth factors (Loirand et al., 2006); hence, KRIT1 and its associated proteins may serve as a physiological brake on vascular leak induced by many agonists. $Krit1^{+/-}$ and $Ccm2^{+/-}$ mice expressed half-normal amounts of their gene products accompanied by defective vascular barrier function in both brain and lung. Heterozygosity-associated vascular leak was reversible by fasudil treatment, demonstrating that the in vitro KRIT1/CCM2→RhoA→ROCK signaling pathway is also operative in preventing vascular leak in vivo. It is possible that a KRIT1/CCM2 deficit-associated leak may contribute to CCM lesion formation. Although $Krit1^{+/-}$ and $Ccm2^{+/-}$ mice mimic the genetic status of human CCM patients, heterozygous mice generally lack CCMs unless they are sensitized by a lack of p53 (Plummer et al., 2004). This lack of lesion formation may be a result of variability in penetrance, as with humans (Plummer et al., 2004; Gianfrancesco et al., 2007; Liquori et al., 2007), or of the shorter lifespan of mice. Our findings raise the possibility that another consequence of $Krit1$ or $Ccm2$ mutations may be a generalized defect in endothelial barrier function.

ROCK1 and 2 are serine/threonine kinases, which contribute to stress fiber formation by inactivating myosin phosphatase and by phosphorylating MLC. pMLC is a regulator of endothelial and SMC contractility, thus playing a central role in vascular tone and function (van Hinsbergh and van Nieuw Amerongen, 2002; Sun et al., 2006). ROCK also activates Lim kinase to inhibit cofilin, which prevents actin depolymerization, and it further increases contractility by directly phosphorylating MLC. Increased contractility can disrupt cell–cell adhesion and contribute to increased vascular permeability (Dudek and Garcia, 2001; Rolfe et al., 2005). ROCK also phosphorylates claudins in tight junctions to regulate permeability of the blood-brain barrier, which is largely composed of tight junctions (Yamamoto et al., 2008). The effect of ROCK on claudins may prove to be of particular interest in CCM disease, wherein lesions are predominantly cerebral, are known to have defective junctional contacts, and are known to leak (Clatterbuck et al., 2001).

Increasing evidence shows that CCM is a largely endothelial disease (Glading et al., 2007; Shenkar et al., 2008a,b; Pagenstecher et al., 2009). We herein related human CCM disease to a ROCK-mediated vascular defect by evaluating human CCM lesions for pMLC. pMLC was present in striking amounts in endothelium of both sporadic and familial human lesions associated with either KRIT1 or CCM2 deficiency. Thus, it is likely that the complete lack of KRIT1 or CCM2 in CCM lesion endothelium leads to excessive activation of RhoA-ROCK signaling, resulting in local hyperpermeability. Our data also raise the possibility that ROCK signaling contributes to other aspects of lesion forma-

tion. ROCK hyperactivation in embryogenesis could contribute to the developmental aortic obstruction seen in both zebrafish and mice (Whitehead et al., 2004; Mably et al., 2006; Malone et al., 2007; Hogan et al., 2008) by producing localized sustained contraction of vascular cells. Alternatively, there may be other effects of KRIT1 deficit, for example, KRIT1 can enter the nucleus; hence, future studies will be needed to ascertain the hierarchy of the complex events that lead to CCM lesion formation. That said, our data point to ROCK signaling as a key player.

Human CCM lesions manifest a robust oligoclonal antigen-driven immune response (Shi et al., 2007, 2009). Radiation exposure can also trigger de novo development of CCM lesions (Jain et al., 2005; Nyáry et al., 2007). The majority of human lesions occur sporadically, in association with preexisting developmental venous anomalies or capillary telangiectasia (Gault et al., 2004, 2006; Al–Shahi Salman et al., 2008). These conditions may contribute to a background of increased vascular permeability, as seen in the heterozygous genetic state, favoring CCM lesion genesis. Our results demonstrate that sporadic human CCMs display excess ROCK activity to the same extent as familial heterozygous CCM2 lesions. ROCK-mediated low level constitutive cerebral vessel hyperpermeability is potentially a critical factor predisposing to both types of lesion genesis.

Long-term treatment of CCM patients with fasudil could prove beneficial in preventing hemorrhagic stroke and deterring formation of new lesions by strengthening cerebral microvascular endothelial stability. Fasudil inhibition of ROCK acts through competitive binding with ATP for a catalytic site. It also inhibits Ca^{2+} sensitization of myosin phosphorylation (Olson, 2008). Fasudil is currently used for cerebral vasospasm treatment in Japan and is well tolerated in man. Moreover, it is currently undergoing human trials in the United States for treatment of pulmonary hypertension and other diseases (Olson, 2008). Our studies suggest that fasudil could also prove beneficial in acute situations of pathological vascular leak (e.g., sepsis) as well as CCM. Support for this idea also comes from recent studies showing that a ROCK inhibitor can ameliorate thrombin or TNF-mediated endothelial permeability in vitro (Mong and Wang, 2009; Satoh et al., 2010). In light of increased leak response of $Krit1^{+/-}$ and $Ccm2^{+/-}$ mice to LPS in this experiment, human CCM patients could have heightened susceptibility to noncerebral vascular pathologies, in which case fasudil could provide additional therapeutic benefit.

MATERIALS AND METHODS

Cell culture. HUVEC (Cambrex) and primary mouse pulmonary endothelial cells were cultured in EGM2 medium (Cambrex), 10% fetal bovine serum, and 1% penicillin/streptomycin (Invitrogen).

siRNA and cDNA. siRNA against human KRIT1 (Applied Biosystems) was previously described (Glading et al., 2007). siRNA against human CCM2 was obtained from Thermo Fisher Scientific. Negative control siRNA having no known human, mouse, or rat gene targets was obtained from Thermo Fisher Scientific. cDNA for hemagglutinin-tagged full length KRIT1 was previously described (Glading et al., 2007). pRK5-CCM2

encoding FLAG-tagged WT human CCM2 has been previously described (Zawistowski et al., 2005). siRNA-resistant silent mutations were constructed for knockdown reconstitution studies. Additional silent mutations in the coding sequence created a vector encoding siRNA-resistant CCM2-F217A, a mutant unable to bind KRIT1 (Zawistowski et al., 2005).

Transfection. HUVEC were transfected using a Nucleofector (Lonza) as previously described (Glading et al., 2007). In brief, 0.5×10^6 cells/transfection were suspended in HUVEC Solution (VPB-1002; Lonza) with 2.5 µg siRNA, with or without 1.5 µg DNA, nucleoporated using program M-003 or A-034, and then plated on fibronectin (FN)-coated culture plates (Falcon), glass coverslips (Corning), or Transwell 3-µm- polyester filters (Corning) as indicated.

Immunoprecipitation and Western blotting. Cells were scraped in lysis buffer (50 mM Tris, 150 mM NaCl, 0.5% NP-40, and 5 mM $MgCl_2$, plus protease-phosphatase inhibitor cocktails; Sigma-Aldrich). Lysates were centrifuged at 14,000 rpm for 10 min, and protein concentrations were determined by BCA assay (Thermo Fisher Scientific). 500 µg of protein was precleared with 25 µl of 50% protein G–Sepharose beads (GE Healthcare), and then supernatants were incubated with 2–5 µg of immunoprecipitating antibody at 4°C with continuous rocking for 2 h. 25 µl of protein G–Sepharose beads were added and incubated overnight at 4°C with continuous rocking. Pellets were centrifuged at 8,000 g for 2 min and washed three times with lysis buffer. Protein was solubilized by heating at 95°C for 5 min in 20 µl SDS-PAGE sample buffer and then fractionated on 4–20% SDS-PAGE. Protein was transferred to nitrocellulose membranes and detected by immunoblotting.

Reagents. Monoclonal anti-KRIT1 (15B2) and polyclonal anti-KRIT1 (6832) antibodies were previously described (Glading et al., 2007). Anti-KRIT1 15B2 was used for immunoprecipitation and immunofluorescence at 1:1,000. Rabbit anti-KRIT1 6832 serum was used for immunoblotting at 1:1,000. Anti-GAPDH (Santa Cruz Biotechnology, Inc.) was used at 1:2,000. Nonimmune mouse and rabbit IgG were obtained from Santa Cruz Biotechnology, Inc. Rabbit and mouse polyclonal anti-CCM2 (Abnova) were used for immunoblotting and immunostaining at 1:1,000 and 1:500, respectively. Anti–phospho [Thr180/Ser19]-MLC antibodies (Cell Signaling Technology) were used for immunoblotting at 1:1,000, immunostaining at 1:500, and immunohistochemistry at 1:250. Rabbit anti-MYPT1 and goat anti–phospho [Thr853]-MYPT1 were obtained from Santa Cruz Biotechnology, Inc. Alexa-conjugated anti-IgG and Alexa-conjugated phalloidin were obtained from Invitrogen. Goat anti–rabbit IgG-biotin antibody was obtained from Vector Laboratories. ROCK inhibitors H-1152, Y27632, and fasudil (5-Isoquinolinesulfonyl homopiperazine, 2HCl) were obtained from EMD. Evans blue dye and all other reagents were obtained from Sigma-Aldrich unless otherwise indicated.

Immunofluorescence. Cells grown to ∼80% percent confluence on FN-coated glass coverslips were fixed with 3.7% formaldehyde for 30 min, permeabilized for 10 min with 0.15% Triton X-100, and blocked for 1 h with 10% normal goat serum (Invitrogen) in TBS-Tween (TBST). Antibodies diluted in TBS were added to coverslips and incubated overnight in a humidified chamber. Coverslips were washed with TBST and then incubated with indicated Alexa-labeled anti-IgG (Invitrogen) at 1:1,000 overnight at 4°C. Coverslips were washed in TBST and then mounted using Prolong Gold (Invitrogen). Imaging was performed by a microscope (LR23; Leica) with a charge-coupled device camera (model 2.2.1; Diagnostic Instruments, Inc.) or a confocal microscopy system (TCS SP2 AOBS with DMRE microscope and HCX PL APO 63×/1.32 oil objective; Leica). Images were acquired for each experiment using the same gamma settings for all samples and processed using Photoshop II software (Adobe).

Endothelial in vitro permeability assay. HUVEC or primary mouse endothelial cells were nucleoporated with indicated siRNA and/or cDNA, plated into 3-µm pore polyester FN-coated Transwell filters (Corning), and

incubated for 48 h at 37°C in 5% CO_2 to full confluence. Medium was replaced with phenol-free DME with 1% serum. In some assays, cells were treated with vehicle or 3 µM ROCK inhibitor H-1152 for 30 min. In control experiments, an alternate ROCK inhibitor, Y27632, was used at 1 µM. 50 µl of phenol-free DME containing 1.5 µg/ml of horseradish peroxidase (Sigma-Aldrich) were added to all filter upper wells for 60 min. In some experiments, 1.5 µg/ml FITC-dextran (44 kD; Sigma-Aldrich) replaced HRP as a label. Filters were removed from outer wells, fixed in 3.5% formaldehyde, and stained with 0.25% Coomassie blue for microscopy to reconfirm the integrity of cell monolayers.

HRP content of lower chamber medium was measured using a microplate peroxidase colorimetric assay as previously described (Glading et al., 2007). A_{490} was acquired and raw absorbance values were normalized as a percentage of control untransfected (vehicle only) cell sample absorbance. For experiments using the FITC-dextran label, 100 µl of lower chamber medium/well in triplicates per sample was analyzed by 96-well microplate fluorimetry. Data from at least three experiments were pooled and analyzed for statistical significance using analysis of variance (ANOVA) with Sigma-Stat software (SPSS). Graph bars indicate means and SE of pooled data. n- and p-values are shown in the figure legends.

Pulmonary endothelial cell isolation. Mouse primary vascular endothelial cells were isolated from tissues by sequential CD45-negative and CD31-positive immunomagnetic bead selection. Animals were perfused with HBSS containing dispase and 0.2% collagenase. Brains, lungs, livers, and kidneys were removed, minced, and further digested in dispase/0.2% collagenase (Sigma-Aldrich). Organs from the same genotype were pooled for collection. A single-cell suspension was prepared by passing digested organs through a 70-µm cell strainer (BD). Cells were incubated with biotinylated rat anti–mouse CD45, washed, and then incubated with anti-biotin microbeads (Miltenyi Biotec). Cells were washed and placed in a microtube in a magnet unit (Invitrogen) to isolate $CD45^+$ cells. CD45-negative cells were collected and labeled with rat anti–mouse CD31 (Invitrogen). Cells were washed, and then anti–rat IgG-coated magnetic beads were added and $CD31^+$ cells were isolated by magnet. Endothelial cell identity was confirmed by FACS for VE-cadherin (Fig. S2). Cells were grown on FN-coated coverslips, cultured in EBM2 medium, or lysed for Western blotting.

Rho activity assay. Cells transfected as described in the Transfection section were plated in FN-coated 60-mm culture dishes concurrent with permeability and immunofluorescence assays and grown for 48 h. Cells were washed with ice-cold HBSS, and then plates were flash frozen on dry ice and stored at −70°C. Frozen cells on plates were scraped with assay lysis buffer (Cytoskeleton, Inc.) and cell lysates clarified by centrifugation for 10 min at 14,000 g at 4°C. Protein content was measured using a DC Protein Assay kit (Bio-Rad Laboratories). Samples containing equal amounts of protein were subjected to either colorimetric or luminescence quantitative microplate enzymeimmunoassay for GTP-bound RhoA according to the manufacturer's direction (Cytoskeleton, Inc). For colorimetric assays, mean sample absorbance at 690 nm, and for luminescent assays, mean sample light units, were normalized to control samples and statistically analyzed by ANOVA as indicated in the figure legends.

Mice. $Krit1^{+/-}$ and $Ccm2^{+/-}$ mice backcrossed onto C57BL/6J background have been previously described (Whitehead et al., 2004; Plummer et al., 2006; provided by D. Marchuk, Duke University, Durham, NC). All experiments performed using mice were in accord with animal procedure protocols approved by the University of California, San Diego Institutional Animal Care and Use Committee.

Evan's blue dye in vivo extravasation and edema assays. $Krit1^{+/-}$ and $Ccm2^{+/-}$ mice were age-matched to WT littermates. Evan's blue (EB) extravasation from blood into interstitial tissue was evaluated as previously described (Reutershan et al., 2007; Stockton et al., 2007). Organs were evaluated for edema as wet weight percentage of total organ weight, as a secondary

index of vascular leak (Ipaktchi et al., 2006; Wilson et al., 2007). In brief, animals were anaesthetized by 3% isoflurane inhalant, weighed, and pretreated for 30 min by intravenous administration of either sterile HBSS vehicle or fasudil at 20 µg/kg mouse, as previously described (Yamashita et al., 2007; Slotta et al., 2008), and EB (500 µg/25 g mouse). After 30 min, mice were treated by intraperitoneal injection with either vehicle or LPS (5 µg/g mouse; Sigma-Aldrich). After 2 h, animals were sacrificed by CO_2 inhalation, and 100 µl of blood was drawn from the right ventricle into heparinized microtubes. The plasma fraction of whole blood was isolated by centrifugation for 10 min at 1,200 g. Perfusion of mice with sterile HBSS cleared vessels of circulating EB. Lungs and brains were removed to tared microtubes in separated halves and placed on dry ice. One lung and one half brain from each animal were weighed using a digital top-loading balance (Mettler Toledo), dried in a heated rotator for 4 h, and then reweighed for a wet/dry weight ratio. The remaining organs were homogenized in PBS with a PowerGen 35 Homogenizer (Thermo Fisher Scientific). EB was extracted from 1 ml of lung homogenate by incubation in 3 ml formamide, and 1 ml of brain homogenate with 2 ml formamide, for 18 h at 70°C. Sample absorbances of extracted organ and plasma EB content at 620 and 740 nm were read on a spectrophotometer (ThermoMax; MDS Analytical Technologies).The corrected absorption of tissue EB at 620 nm was calculated using the equation Corrected A_{620} = actual A_{620} − [$1.426(A_{740})$ + 0.03], as previously described (Reutershan et al., 2007). EB concentration was calculated by inverse prediction of the regression equation of a standard curve. The EB concentration in micrograms per milliliter was converted to micrograms per gram of wet weight of lungs.

Immunohistochemistry and human lesion samples. Cerebral lesion specimens and genotyping information were obtained from CCM surgical patients at the North Shore University Health System in a manner consistent with institutional review board protocols and National Institutes of Health human subject regulations. All human CCM lesions were excised from adults for surgical indications unrelated to this research, as was control brain tissue resected in the course of epilepsy surgery. Paraffin-embedded 5-µm tissue sections were deparaffinized by serial washing in xylenes and then ethanol dilutions (100, 95, and 70%). Endogenous peroxidase was neutralized by 3% H_2O_2 in methanol for 30 min. Antigen retrieval was performed using citrate-buffered antigen retrieval solution (Vector Laboratories). Sections were blocked using PBS-FSGO (PBS supplemented with 0.5% fish skin gelatin [FSGO]; Sigma-Aldrich) and 5% goat serum (Invitrogen) and biotin-blocked using a kit (Vector Laboratories). Slides were probed with primary antibody (1:250) against KRIT1, CCM2, or phospho-MLC in PBS-FSGO as described in Immunofluorescence. Control sections were treated with rabbit or mouse IgG (Santa Cruz Biotechnology, Inc.). All primary antibody incubations were performed overnight at 4°C. Slides were washed and probed with biotinylated goat anti–rabbit or anti–mouse IgG (Vector Laboratories) at 1:400 for 2 h at room temperature and then washed in PBS-FSGO and incubated with Elite ABC kit reagents (Vector Laboratories) for 30 min at room temperature. Color was developed using DAB (3,3′-diaminobenzidine) as a substrate for 5 min. Slides were washed and counterstained with hematoxylin, mounted with Vectashield, and photographed using a bright-field microscope (Leica) with a camera (CCM; Diagnostic Instruments).

Statistical analysis. For all quantitative assays, data from at least three experiments were analyzed for statistical significance by ANOVA with a Holm-Sidak multiple comparison test, using SigmaStat analytical software (Jandel Scientific), and are shown graphically as means ± SE. Photographic or Western blot images shown are representative of results seen consistently in three or more experiments.

Online supplemental material. Fig. S1 shows that ROCK activation in HUVEC treated with KRIT1 or CCM2 siRNA increases phosphorylation of MYPT1, reversible by ROCK inhibitor Y27632. Fig. S2 shows Krit and Ccm2 mouse EC isolation efficacy by VE-cadherin FACS and densitometry of immunoblotting against pMLC in isolated EC. Fig. S3 shows CCM human

lesion expression of KRIT1 and CCM2 protein. Online supplemental material is available at http://www.jem.org/cgi/content/full/jem.20091258.

REFERENCES

Akers, A.L., E. Johnson, G.K. Steinberg, J.M. Zabramski, and D.A. Marchuk. 2009. Biallelic somatic and germline mutations in cerebral cavernous malformations (CCMs): evidence for a two-hit mechanism of CCM pathogenesis. *Hum. Mol. Genet.* 18:919–930.

Al-Shahi Salman, R., M.J. Berg, L. Morrison, and I.A. Awad; Angioma Alliance Scientific Advisory Board. 2008. Hemorrhage from cavernous malformations of the brain: definition and reporting standards. *Stroke.* 39:3222–3230. doi:10.1161/STROKEAHA.108.515544

Ardeshiri, A., A. Ardeshiri, A. Beiras-Fernandez, O.K. Steinlein, and P.A. Winkler. 2008. Multiple cerebral cavernous malformations associated with extracranial mesenchymal anomalies. *Neurosurg. Rev.* 31:11–17. doi:10.1007/s10143-007-0111-7

Awad, I.A. 2005. Unfolding knowledge on cerebral cavernous malformations. *Surg. Neurol.* 63:317–318. doi:10.1016/j.surneu.2004.12.032

Berridge, M.J. 2008. Smooth muscle cell calcium activation mechanisms. *J. Physiol.* 586:5047–5061. doi:10.1113/jphysiol.2008.160440

Boulday, G., A. Blécon, N. Petit, F. Chareyre, L.A. Garcia, M. Niwa-Kawakita, M. Giovannini, and E. Tournier-Lasserve. 2009. Tissue-specific conditional CCM2 knockout mice establish the essential role of endothelial CCM2 in angiogenesis: implications for human cerebral cavernous malformations. *Dis Model Mech.* 2:168–177. doi:10.1242/dmm.001263

Clatterbuck, R.E., C.G. Eberhart, B.J. Crain, and D. Rigamonti. 2001. Ultrastructural and immunocytochemical evidence that an incompetent blood-brain barrier is related to the pathophysiology of cavernous malformations. *J. Neurol. Neurosurg. Psychiatry.* 71:188–192. doi:10.1136/jnnp.71.2.188

Crose, L.E., T.L. Hilder, N. Sciaky, and G.L. Johnson. 2009. Cerebral cavernous malformation 2 protein promotes smad ubiquitin regulatory factor 1-mediated RhoA degradation in endothelial cells. *J. Biol. Chem.* 284:13301–13305. doi:10.1074/jbc.C900009200

Cullere, X., S.K. Shaw, L. Andersson, J. Hirahashi, F.W. Luscinskas, and T.N. Mayadas. 2005. Regulation of vascular endothelial barrier function by Epac, a cAMP-activated exchange factor for Rap GTPase. *Blood.* 105:1950–1955. doi:10.1182/blood-2004-05-1987

Dudek, S.M., and J.G.N. Garcia. 2001. Cytoskeletal regulation of pulmonary vascular permeability. *J. Appl. Physiol.* 91:1487–1500.

Fong, B., P.H. Watson, and A.J. Watson. 2007. Mouse preimplantation embryo responses to culture medium osmolarity include increased expression of CCM2 and p38 MAPK activation. *BMC Dev. Biol.* 7:2. doi:10.1186/1471-213X-7-2

Gault, J., H. Sarin, N.A. Awadallah, R. Shenkar, and I.A. Awad. 2004. Pathobiology of human cerebrovascular malformations: basic mechanisms and clinical relevance. *Neurosurgery.* 55:1–16. doi:10.1227/01.NEU.0000126872.23715.E5

Gault, J., S. Sain, L.J. Hu, and I.A. Awad. 2006. Spectrum of genotype and clinical manifestations in cerebral cavernous malformations. *Neurosurgery.* 59:1278–1284. doi:10.1227/01.NEU.0000249188.38409.03

Gavard, J., and J.S. Gutkind. 2006. VEGF controls endothelial-cell permeability by promoting the beta-arrestin-dependent endocytosis of VE-cadherin. *Nat. Cell Biol.* 8:1223–1234. doi:10.1038/ncb1486

Gianfrancesco, F., M. Cannella, T. Martino, V. Maglione, T. Esposito, G. Innocenzi, E. Vitale, C.L. Liquori, D.A. Marchuk, and F. Squitieri. 2007. Highly variable penetrance in subjects affected with cavernous

cerebral angiomas (CCM) carrying novel CCM1 and CCM2 mutations. *Am. J. Med. Genet. B. Neuropsychiatr. Genet.* 144B:691–695. doi:10.1002/ajmg.b.30381

Glading, A., J. Han, R.A. Stockton, and M.H. Ginsberg. 2007. KRIT-1/CCM1 is a Rap1 effector that regulates endothelial cell–cell junctions. *J. Cell Biol.* 179:247–254. doi:10.1083/jcb.200705175

Hilder, T.L., M.H. Malone, S. Bencharit, J. Colicelli, T.A. Haystead, G.L. Johnson, and C.C. Wu. 2007a. Proteomic identification of the cerebral cavernous malformation signaling complex. *J. Proteome Res.* 6:4343–4355. doi:10.1021/pr0704276

Hilder, T.L., M.H. Malone, and G.L. Johnson. 2007b. Hyperosmotic induction of mitogen-activated protein kinase scaffolding. *Methods Enzymol.* 428:297–312. doi:10.1016/S0076-6879(07)28017-6

Hogan, B.M., J. Bussmann, H. Wolburg, and S. Schulte-Merker. 2008. ccm1 cell autonomously regulates endothelial cellular morphogenesis and vascular tubulogenesis in zebrafish. *Hum. Mol. Genet.* 17:2424–2432. doi:10.1093/hmg/ddn142

Ipaktchi, K., A. Mattar, A.D. Niederbichler, L.M. Hoesel, S. Vollmannshauser, M.R. Hemmila, G.L. Su, D.G. Remick, S.C. Wang, and S. Arbabi. 2006. Attenuating burn wound inflammatory signaling reduces systemic inflammation and acute lung injury. *J. Immunol.* 177:8065–8071.

Jain, R., P.L. Robertson, D. Gandhi, S.K. Gujar, K.M. Muraszko, and S. Gebarski. 2005. Radiation-induced cavernomas of the brain. *AJNR Am. J. Neuroradiol.* 26:1158–1162.

Kleaveland, B., X. Zheng, J.J. Liu, Y. Blum, J.J. Tung, Z. Zou, S.M. Sweeney, M. Chen, L. Guo, M.M. Lu, et al. 2009. Regulation of cardiovascular development and integrity by the heart of glass-cerebral cavernous malformation protein pathway. *Nat. Med.* 15:169–176. doi:10.1038/nm.1918

Kooistra, M.R., M. Corada, E. Dejana, and J.L. Bos. 2005. Epac1 regulates integrity of endothelial cell junctions through VE-cadherin. *FEBS Lett.* 579:4966–4972. doi:10.1016/j.febslet.2005.07.080

Liquori, C.L., M.J. Berg, A.M. Siegel, E. Huang, J.S. Zawistowski, T. Stoffer, D. Verlaan, F. Balogun, L. Hughes, T.P. Leedom, et al. 2003. Mutations in a gene encoding a novel protein containing a phosphotyrosine-binding domain cause type 2 cerebral cavernous malformations. *Am. J. Hum. Genet.* 73:1459–1464. doi:10.1086/380314

Liquori, C.L., M.J. Berg, F. Squitieri, T.P. Leedom, L. Ptacek, E.W. Johnson, and D.A. Marchuk. 2007. Deletions in CCM2 are a common cause of cerebral cavernous malformations. *Am. J. Hum. Genet.* 80:69–75. doi:10.1086/510439

Loirand, G., P. Guérin, and P. Pacaud. 2006. Rho kinases in cardiovascular physiology and pathophysiology. *Circ. Res.* 98:322–334. doi:10.1161/01.RES.0000201960.04223.3c

Mably, J.D., L.P. Chuang, F.C. Serluca, M.-A.P.K. Mohideen, J.-N. Chen, and M.C. Fishman. 2006. santa and valentine pattern concentric growth of cardiac myocardium in the zebrafish. *Development.* 133:3139–3146. doi:10.1242/dev.02469

Malone, M.H., N. Sciaky, L. Stalheim, K.M. Hahn, E. Linney, and G.L. Johnson. 2007. Laser-scanning velocimetry: a confocal microscopy method for quantitative measurement of cardiovascular performance in zebrafish embryos and larvae. *BMC Biotechnol.* 7:40. doi:10.1186/1472-6750-7-40

Mong, P.Y., and Q. Wang. 2009. Activation of Rho kinase isoforms in lung endothelial cells during inflammation. *J. Immunol.* 182:2385–2394. doi:10.4049/jimmunol.0802811

Nyáry, I., O. Major, Z. Hanzély, and G.T. Szeifert. 2007. Pathological considerations to irradiation of cavernous malformations. *Prog. Neurol. Surg.* 20:231–234.

Olson, M.F. 2008. Applications for ROCK kinase inhibition. *Curr. Opin. Cell Biol.* 20:242–248. doi:10.1016/j.ceb.2008.01.002

Pagenstecher, A., S. Stahl, U. Sure, and U. Felbor. 2009. A two-hit mechanism causes cerebral cavernous malformations: complete inactivation of CCM1, CCM2 or CCM3 in affected endothelial cells. *Hum. Mol. Genet.* 18:911–918.

Petit, N., A. Blécon, C. Denier, and E. Tournier-Lasserve. 2006. Patterns of expression of the three cerebral cavernous malformation (CCM) genes during embryonic and postnatal brain development. *Gene Expr. Patterns.* 6:495–503. doi:10.1016/j.modgep.2005.11.001

Plummer, N.W., C.J. Gallione, S. Srinivasan, J.S. Zawistowski, D.N. Louis, and D.A. Marchuk. 2004. Loss of p53 sensitizes mice with a mutation in Ccm1 (KRIT1) to development of cerebral vascular malformations. *Am. J. Pathol.* 165:1509–1518.

Plummer, N.W., J.S. Zawistowski, and D.A. Marchuk. 2005. Genetics of cerebral cavernous malformations. *Curr. Neurol. Neurosci. Rep.* 5:391–396. doi:10.1007/s11910-005-0063-7

Plummer, N.W., T.L. Squire, S. Srinivasan, E. Huang, J.S. Zawistowski, H. Matsunami, L.P. Hale, and D.A. Marchuk. 2006. Neuronal expression of the Ccm2 gene in a new mouse model of cerebral cavernous malformations. *Mamm. Genome.* 17:119–128. doi:10.1007/s00335-005-0098-8

Reutershan, J., R. Stockton, A. Zarbock, G.W. Sullivan, D. Chang, D. Scott, M.A. Schwartz, and K. Ley. 2007. Blocking p21-activated kinase reduces lipopolysaccharide-induced acute lung injury by preventing polymorphonuclear leukocyte infiltration. *Am. J. Respir. Crit. Care Med.* 175:1027–1035. doi:10.1164/rccm.200612-1822OC

Rolfe, B.E., N.F. Worth, C.J. World, J.H. Campbell, and G.R. Campbell. 2005. Rho and vascular disease. *Atherosclerosis.* 183:1–16. doi:10.1016/j.atherosclerosis.2005.04.023

Sahoo, T., E.W. Johnson, J.W. Thomas, P.M. Kuehl, T.L. Jones, C.G. Dokken, J.W. Touchman, C.J. Gallione, S.Q. Lee-Lin, B. Kosofsky, et al. 1999. Mutations in the gene encoding KRIT1, a Krev-1/rap1a binding protein, cause cerebral cavernous malformations (CCM1). *Hum. Mol. Genet.* 8:2325–2333. doi:10.1093/hmg/8.12.2325

Satoh, S., A. Hitomi, I. Ikegaki, K. Kawasaki, O. Nakazono, M. Iwasaki, M. Mohri, and T. Asano. 2010. Amelioration of endothelial damage/dysfunction is a possible mechanism for the neuroprotective effects of Rho-kinase inhibitors against ischemic brain damage. *Brain Res. Bull.* 81:191–195. doi:10.1016/j.brainresbull.2009.08.021

Seker, A., K.L. Pricola, B. Guclu, A.K. Ozturk, A. Louvi, and M. Gunel. 2006. CCM2 expression parallels that of CCM1. *Stroke.* 37:518–523. doi:10.1161/01.STR.0000198835.49387.25

Serebriiskii, I., J. Estojak, G. Sonoda, J.R. Testa, and E.A. Golemis. 1997. Association of Krev-1/rap1a with Krit1, a novel ankyrin repeat-containing protein encoded by a gene mapping to 7q21-22. *Oncogene.* 15:1043–1049. doi:10.1038/sj.onc.1201268

Shenkar, R., P.N. Venkatasubramanian, A.M. Wyrwicz, J.C. Zhao, C. Shi, A. Akers, D.A. Marchuk, and I.A. Awad. 2008a. Advanced magnetic resonance imaging of cerebral cavernous malformations: part II. Imaging of lesions in murine models. *Neurosurgery.* 63:790–797. doi:10.1227/01.NEU.0000315862.24920.49

Shenkar, R., P.N. Venkatasubramanian, J.C. Zhao, H.H. Batjer, A.M. Wyrwicz, and I.A. Awad. 2008b. Advanced magnetic resonance imaging of cerebral cavernous malformations: part I. High-field imaging of excised human lesions. *Neurosurgery.* 63:782–789. doi:10.1227/01.NEU.0000325490.80694.A2

Shi, C., R. Shenkar, H.H. Batjer, I.J. Check, and I.A. Awad. 2007. Oligoclonal immune response in cerebral cavernous malformations. Laboratory investigation. *J. Neurosurg.* 107:1023–1026. doi:10.3171/JNS-07/11/1023

Shi, C., R. Shenkar, H. Du, E. Duckworth, H. Raja, H.H. Batjer, and I.A. Awad. 2009. Immune response in human cerebral cavernous malformations. *Stroke.* 40:1659–1665. doi:10.1161/STROKEAHA.108.538769

Shimokawa, H., and A. Takeshita. 2005. Rho-kinase is an important therapeutic target in cardiovascular medicine. *Arterioscler. Thromb. Vasc. Biol.* 25:1767–1775. doi:10.1161/01.ATV.0000176193.83629.c8

Slotta, J.E., O.O. Braun, M.D. Menger, and H. Thorlacius. 2008. Central role of rho kinase in lipopolysaccharide–induced platelet capture on venous endothelium. *J. Investig. Med.* 56:720–725.

Stockton, R.A., E. Schaefer, and M.A. Schwartz. 2004. p21-activated kinase regulates endothelial permeability through modulation of contractility. *J. Biol. Chem.* 279:46621–46630. doi:10.1074/jbc.M408877200

Stockton, R., J. Reutershan, D. Scott, J. Sanders, K. Ley, and M.A. Schwartz. 2007. Induction of vascular permeability: beta PIX and GIT1 scaffold the activation of extracellular signal–regulated kinase by PAK. *Mol. Biol. Cell.* 18:2346–2355. doi:10.1091/mbc.E06-07-0584

Sun, H., J.W. Breslin, J. Zhu, S.Y. Yuan, and M.H. Wu. 2006. Rho and ROCK signaling in VEGF-induced microvascular endothelial hyperpermeability. *Microcirculation*. 13:237–247. doi:10.1080/10739680600556944

Tan, W., T.R. Palmby, J. Gavard, P. Amornphimoltham, Y. Zheng, and J.S. Gutkind. 2008. An essential role for Rac1 in endothelial cell function and vascular development. *FASEB J*. 22:1829–1838. doi:10.1096/fj.07-096438

Uhlik, M.T., A.N. Abell, N.L. Johnson, W. Sun, B.D. Cuevas, K.E. Lobel-Rice, E.A. Horne, M.L. Dell'Acqua, and G.L. Johnson. 2003. Rac-MEKK3-MKK3 scaffolding for p38 MAPK activation during hyperosmotic shock. *Nat. Cell Biol*. 5:1104–1110. doi:10.1038/ncb1071

van Hinsbergh, V.W., and G.P. van Nieuw Amerongen. 2002. Intracellular signalling involved in modulating human endothelial barrier function. *J. Anat*. 200:549–560. doi:10.1046/j.1469-7580.2002.00060.x

van Wetering, S., J.D. van Buul, S. Quik, F.P.J. Mul, E.C. Anthony, J.P. ten Klooster, J.G. Collard, and P.L. Hordijk. 2002. Reactive oxygen species mediate Rac-induced loss of cell-cell adhesion in primary human endothelial cells. *J. Cell Sci*. 115:1837–1846.

Voss, K., S. Stahl, E. Schleider, S. Ullrich, J. Nickel, T.D. Mueller, and U. Felbor. 2007. CCM3 interacts with CCM2 indicating common pathogenesis for cerebral cavernous malformations. *Neurogenetics*. 8:249–256. doi:10.1007/s10048-007-0098-9

Whitehead, K.J., N.W. Plummer, J.A. Adams, D.A. Marchuk, and D.Y. Li. 2004. Ccm1 is required for arterial morphogenesis: implications for the etiology of human cavernous malformations. *Development*. 131:1437–1448. doi:10.1242/dev.01036

Whitehead, K.J., A.C. Chan, S. Navankasattusas, W. Koh, N.R. London, J. Ling, A.H. Mayo, S.G. Drakos, C.A. Jones, W. Zhu, et al. 2009. The cerebral cavernous malformation signaling pathway promotes vascular integrity via Rho GTPases. *Nat. Med*. 15:177–184. doi:10.1038/nm.1911

Wilson, M.R., M.E. Goddard, K.P. O'Dea, S. Choudhury, and M. Takata. 2007. Differential roles of p55 and p75 tumor necrosis factor receptors on stretch-induced pulmonary edema in mice. *Am. J. Physiol. Lung Cell. Mol. Physiol*. 293:L60–L68. doi:10.1152/ajplung.00284.2006

Wittchen, E.S., R.A. Worthylake, P. Kelly, P.J. Casey, L.A. Quilliam, and K. Burridge. 2005. Rap1 GTPase inhibits leukocyte transmigration by promoting endothelial barrier function. *J. Biol. Chem*. 280:11675–11682. doi:10.1074/jbc.M412595200

Wójciak-Stothard, B., S. Potempa, T. Eichholtz, and A.J. Ridley. 2001. Rho and Rac but not Cdc42 regulate endothelial cell permeability. *J. Cell Sci*. 114:1343–1355.

Wójciak-Stothard, B., L.Y.F. Tsang, and S.G. Haworth. 2005. Rac and Rho play opposing roles in the regulation of hypoxia/reoxygenation-induced permeability changes in pulmonary artery endothelial cells. *Am. J. Physiol. Lung Cell. Mol. Physiol*. 288:L749–L760. doi:10.1152/ajplung.00361.2004

Yamamoto, M., S.H. Ramirez, S. Sato, T. Kiyota, R.L. Cerny, K. Kaibuchi, Y. Persidsky, and T. Ikezu. 2008. Phosphorylation of claudin-5 and occludin by rho kinase in brain endothelial cells. *Am. J. Pathol*. 172:521–533. doi:10.2353/ajpath.2008.070076

Yamashita, K., Y. Kotani, Y. Nakajima, M. Shimazawa, S. Yoshimura, S. Nakashima, T. Iwama, and H. Hara. 2007. Fasudil, a Rho kinase (ROCK) inhibitor, protects against ischemic neuronal damage in vitro and in vivo by acting directly on neurons. *Brain Res*. 1154:215–224. doi:10.1016/j.brainres.2007.04.013

Zawistowski, J.S., L. Stalheim, M.T. Uhlik, A.N. Abell, B.B. Ancrile, G.L. Johnson, and D.A. Marchuk. 2005. CCM1 and CCM2 protein interactions in cell signaling: implications for cerebral cavernous malformations pathogenesis. *Hum. Mol. Genet*. 14:2521–2531. doi:10.1093/hmg/ddi256

Zhang, J., D. Rigamonti, H.C. Dietz, and R.E. Clatterbuck. 2007. Interaction between krit1 and malcavernin: implications for the pathogenesis of cerebral cavernous malformations. *Neurosurgery*. 60:353–359. doi:10.1227/01.NEU.0000249268.11074.83